Buseckite, (Fe,Zn,Mn)S, a new mineral from the Zakłodzie meteorite

Chi Ma,* John R. Beckett, and George R. Rossman

Division of Geological and Planetary Sciences, California Institute of Technology, Pasadena, California 91125, U.S.A.

Abstract

Buseckite (IMA 2011-070), (Fe,Zn,Mn)S, is the Fe-dominant analog of wurtzite, a new member of the wurtzite group discovered in Zakłodzie, and an ungrouped enstatite-rich achondrite. The type material occurs as single-crystal grains (4–20 μm in size) in contact with two or more of enstatite, plagioclase, troilite, tridymite, quartz, and sinoite. Low-Ni iron, martensitic iron, schreibersite, keilite, cristobalite, and graphite, which are also present in the type sample, are not observed to be in contact with buseckite. Buseckite is black under diffuse illumination and nearly opaque grayish brown in transmitted light. The mean chemical composition of buseckite, as determined by electron microprobe analysis of the type material, is (wt%) S 35.84, Fe 28.68, Zn 23.54, Mn 10.04, Mg 1.18, sum 99.28, leading to an empirical formula calculated on the basis of 2 atoms of $(Fe_{0.46}Zn_{0.32}Mn_{0.16}Mg_{0.04})_{\Sigma0.99}S_{1.01}$. Electron backscatter diffraction patterns of buseckite are a good match to that of synthetic $(Zn_{0.558}Fe_{0.442})S$ with the $P6_3mc$ structure, showing $a = 3.8357$, $c = 6.3002$ Å, $V = 80.27$ Å^3, and $Z = 2$. Buseckite is likely derived from the breakdown of high-temperature pyrrhotite to form troilite and buseckite following the solidification of sulfide-rich liquids produced during impact melting of an enstatite-rich rock.

Keywords: Buseckite, (Fe,Zn,Mn)S, new mineral, wurtzite group, sinoite, Zakłodzie meteorite, enstatite achondrite

Introduction

The Zakłodzie meteorite, which is a moderately weathered find discovered near the village of Zakłodzie, Poland, is an ungrouped enstatite-rich achondrite that has been ascribed to an impact melt (e.g., Keil 2010) and to internal melting within the parent body (Przylibski et al. 2005). During a nano-mineralogy investigation of this meteorite, a new Fe-dominant monosulfide mineral, (Fe,Zn,Mn)S with a $P6_3mc$ wurtzite-type structure, was identified and named "buseckite." Field-emission scanning electron microscope, electron-backscatter diffraction (EBSD), electron microprobe, and micro-Raman spectroscopic analyses were used to characterize its composition and structure and those of associated minerals. All of the minerals in this study were identified structurally with EBSD and/or Raman. (Fe,Zn,Mn)S phases similar in composition to buseckite were previously found through electron microprobe analysis of sulfides in the Yilmia EL6 chondrite (Buseck and Holdsworth 1972), the Grein 002 EL4/5 chondrite (Patzer et al. 2004), and the Zakłodzie achondrite (on a different sample; Karwowski et al. 2007). This study reports the first confirmed (Fe,Zn,Mn)S mineral with the $P6_3mc$ wurtzite-type structure and considers the origin of this phase, relationships to coexisting minerals, and implications through its formation and survival for the evolution of the Zakłodzie meteorite. Preliminary results are given in Ma et al. (2012).

Mineral name and type material

The new mineral and its name have been approved by the Commission on New Minerals, Nomenclature and Classification of the International Mineralogical Association (IMA 2011-070) (Ma 2011). The name is in honor of Peter R. Buseck (b. 1935),

a mineralogist at the Arizona State University, for his many contributions to mineralogy, meteorite research, and transmission electron microscopy. Two Caltech sections, ZAK-TS1 (purchased) and ZAK-TS2 (made at Caltech), taken from facing slices of the meteorite, contain the type material. ZAK-TS2, hereafter referred to as USNM 7607, has been deposited in the Smithsonian Institution's National Museum of Natural History, Washington, D.C., and cataloged under USNM 7607.

## Appearance, physical and optical properties

The type material appears to consist of 11 single-crystal grains scattered in USNM 7607 and ZAK-TS1 along grain boundaries between two or more of enstatite, plagioclase, quartz, and tridymite, absent other sulfides or adjacent to troilite (Figs. 1–3). One of the type grains contains euhedral sinoite (Si_2N_2O) crystals (Fig. 3a). Buseckite (Figs. 1–3) is irregular to subhedral, 4–20 μm in diameter. No forms or twinning were observed.

The Zakłodzie meteorite is a modestly weathered find but each of the 11 buseckite grains that we observed is surrounded by a rim of secondary Fe oxyhydroxides, which also fill fractures that cut across the grains. Buseckite is black under diffuse illumination and nearly opaque grayish brown in transmitted light. Luster, streak, hardness, tenacity, cleavage, fracture, and optical properties, none of which were determined for buseckite because of the small grain size, are likely close to those of wurtzite (Zn,Fe)S. The density, calculated from the empirical formula, is 3.697 g/cm^3. The crystal is non-fluorescent under the electron beam in an SEM.

## Chemical composition

Quantitative elemental microanalyses were conducted with a JEOL 8200 electron microprobe operated at 15 kV and 10 nA in a focused beam mode. Standards for the analysis were syn-
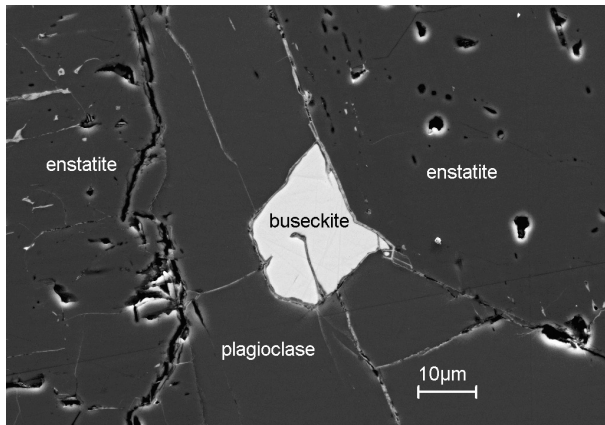
FIGURE 1. Secondary electron image (by an Everhart-Thornley detector) showing a buseckite grain with plagioclase and enstatite. Vein material surrounding and intruding into the buseckite consists of ferric oxy-hydroxides.
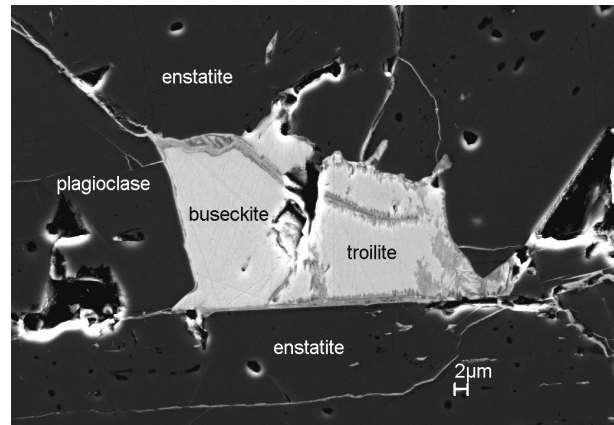
FIGURE 2. Secondary electron image showing buseckite with troilite, plagioclase, and enstatite. Vein material surrounding and intruding into the buseckite consists of ferric oxy-hydroxides.
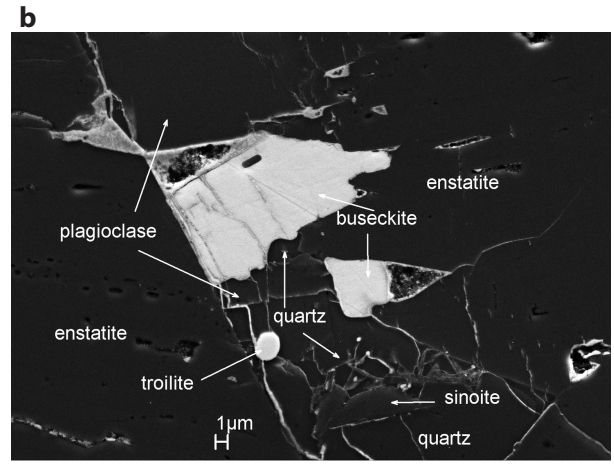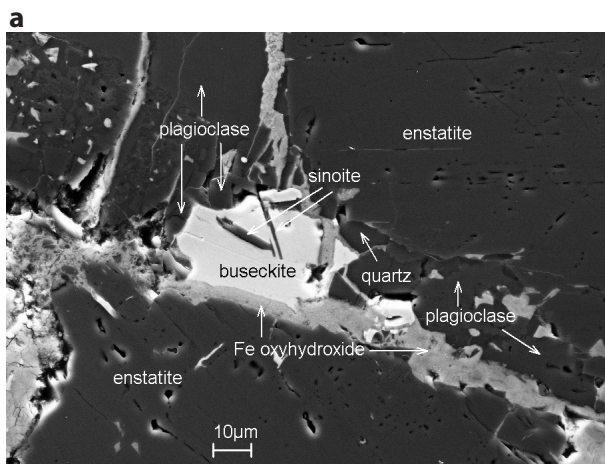
FIGURE 3. Secondary electron images showing (**a**) buseckite with sinoite inclusions and (**b**) buseckite with nearby sinoite.

thetic FeS (Fe$K\alpha$, S$K\alpha$), ZnS (Zn$K\alpha$), MnS (Mn$K\alpha$), forsterite (Mg$K\alpha$), Cr$_2$O$_3$ (Cr$K\alpha$), TiO$_2$ (Ti$K\alpha$), and anorthite (Ca$K\alpha$). Analyses were processed with the CITZAF correction procedure of Armstrong (1995). The average of 14 individual analyses from six grains of the type buseckite reported in Table 1 were carried out using WDS mode. The empirical formula, based on 2 atoms per formula unit, is: (Fe$_{0.46}$Zn$_{0.32}$Mn$_{0.16}$Mg$_{0.04}$)$_{\Sigma 0.99}$S$_{1.01}$, yielding a simplified formula of (Fe,Zn,Mn)S. We observed no significant grain-to-grain differences in buseckite composition and no evidence for zoning within individual grains.

In Figure 4, we show the compositions of Zn-enriched monosulfides from enstatite-enriched meteorites. Note that most of the plotted analyses are consistent with one of the Fe-dominant phases buseckite or rudashevskyite rather than one of the Zn-dominant phases, wurtzite or sphalerite. Compositions of rudashevskyite from the EH4 enstatite chondrite Indarch (Britvin et al. 2008) and the compositions of structurally uncharacterized sulfides from other EH3-4 chondrites plotted in Figure 4 (open circles and diamonds) are similarly Mn-Mg poor. As discussed below, it seems likely that all of these grains have a sphalerite structure

and are either rudashevskyites (Fe dominant) or sphalerites (Zn dominant) depending on Fe/Zn. Buseckite from Zakłodzie has substantially more Mn than known rudashevskyites and the compositions, therefore, plot in the interior of the ternary shown in Figure 4, as do Zn-enriched sulfide compositions from EL4-6 chondrites. The structures of these EL4-6 phases have not been determined but, as discussed below, it is likely that many, if not all, have the wurtzite structure and are, therefore, buseckites. We are aware of no reports of Zn-rich monosulfides in enstatite achondrites (aubrites), presumably reflecting the lower bulk Zn in these meteorites and the presence of daubréelite, which can accommodate considerable Zn (Lin and El Goresy 2002; Keil 2010).

CRYSTALLOGRAPHY

Crystallography by EBSD at a sub-micrometer scale was carried out using methods described in Ma and Rossman (2008, 2009) with an HKL EBSD system on a ZEISS 1550VP scanning electron microscope operated at 20 kV and 6 nA in a focused beam with a 70° tilted stage and in a variable pressure mode (25 Pa). The structure was determined and cell constants obtained

TABLE 1. Mean electron microprobe analytical results for the type buseckite, along with keilite and troilite

Constituent	Buseckite	Troilite (next to buseckite)	Keilite	Troilite (next to keilite)	Troilite (isolated)
wt%	n = 14*	n = 5	n = 6	n = 6	n = 4
S	35.84(21)†	37.65(17)	39.50(22)	37.64(21)	37.44(6)
Fe	28.68(26)	56.46(44)	29.90(22)	56.23(14)	56.03(87)
Zn	23.54(25)	b.d.	0.15(6)	b.d.	b.d.
Mn	10.04(12)	1.18(12)	24.03(12)	1.32(14)	1.40(58)
Mg	1.18(4)	b.d.	4.86(7)	b.d.	b.d.
Cr	b.d.‡	3.83(3)	1.13(4)	4.31(8)	4.13(10)
Ti	b.d.	1.06(7)	b.d.	0.75(4)	0.76(3)
Ca	b.d.	b.d.	0.88(2)	b.d.	b.d.
Ni	b.d.	0.11(4)	b.d.	0.12(3)	0.13(4)
Total	99.28	100.29	100.45	100.37	99.89

* Number of analyses.
† Numbers in parentheses represent one standard deviation of the mean for the n analyses conducted on the phase.
‡ Below detection. Detection limits at 99% confidence are Cr 0.086 wt%, Ti 0.050%, Ca 0.016%, Ni 0.071%, Zr 0.148%, and Mg 0.043%.
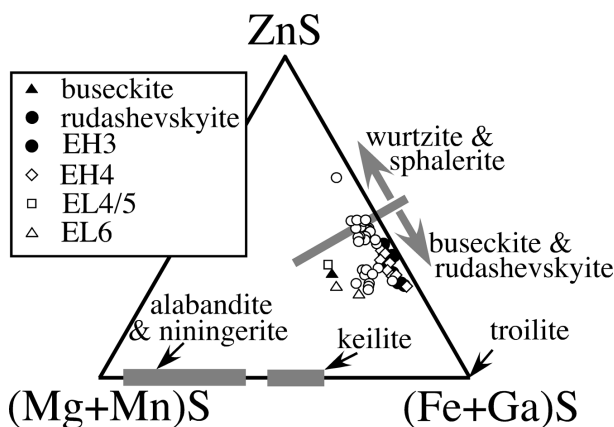
FIGURE 4. Zinc enriched monosulfides from enstatite-rich meteorites plotted in terms of the ternary (Fe+Ga)S-ZnS-(Mg,Mn)S (molar basis). A gray line cutting across the FeS-MnS join separates Fe-dominant from Zn-dominant minerals, keeping in mind that some grains have significant amounts of Ga. Fields for alabandite, niningerite, and keilite taken from a compilation of the literature are also shown. Rudashevskyite compositions, all of which are from Indarch (EH4), are from Britvin et al. (2008); the buseckite composition is from this study. For the other Zn-rich monosulfides (Buseck and Holdsworth 1972; El Goresy and Ehlers 1989; Ikeda 1989; Kissin 1989; Lin and El Goresy 2002; Patzer et al. 2004; Rambaldi et al. 1986), the structures are unknown, so the analyzed phases cannot be assigned a specific mineral name.

by testing the experimental EBSD pattern against the structures of wurtzite, rudashevskyite, keilite, troilite, and pentlandite.

The EBSD patterns (e.g., Fig. 5) can only be indexed using the hexagonal wurtzite structure and this yields a best fit based on unit-cell data for synthetic $(Zn_{0.558}Fe_{0.442})S$ (Kullerud 1953). Buseckite has a hexagonal close packed structure, space group 186: $P6_3mc$, showing $a = 3.8357$, $c = 6.3002$ Å, $V = 80.27$ Å^3, and $Z = 2$, with a mean angular deviation of 0.46. Note that we give no errors on the cell parameters because they are taken directly from the data of the matching synthetic phase in Kullerud (1953).

X-ray powder-diffraction data (Cu$K\alpha_1$) were calculated from the cell parameters of Kullerud (1953) and the empirical formula of the type buseckite from this study using Powder Cell version 2.4 (2000). The strongest X-ray powder diffraction lines are [d in Å, (I), hkl] 3.322 (100) (100), 3.150 (62) (002), 2.938 (90) (101), 2.286 (36) (102), 1.918 (76) (110), 1.775 (76) (103), 1.638 (48) (112), 1.078 (28) (213).

RAMAN SPECTROSCOPY

Raman micro-analysis of buseckite and associated phases was carried out using a Renishaw M1000 micro-Raman spectrometer system and a 514.5 nm laser with the methods described in Ma and Rossman (2008, 2009). A Raman spectrum of buseckite was obtained from 4000 to 100 cm^{-1}. Because some decomposition was visually noted on the sample when the sample was illuminated at the highest laser power, the spectrum was obtained at 25% of full power (corresponding to about 1.2 mW at the sample with the 100× objective). The main feature in the baseline corrected spectrum is a band at 296 cm^{-1} that is asymmetric with a second overlapping component at about 322 cm^{-1} (Fig. 6a). No Raman features were observed between 4000 and 800 cm^{-1}. The spectrum differs from those of rudashevskyite, troilite, and keilite (Fig. 6a). All four of these Fe-dominant sulfides produce comparatively weak Raman spectra.
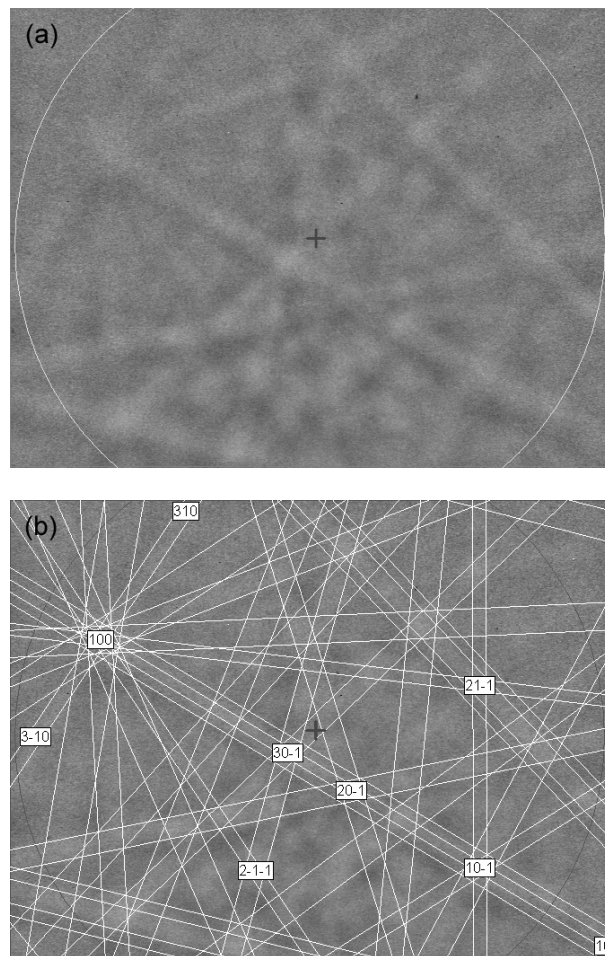
FIGURE 5. (**a**) EBSD pattern of the buseckite crystal in Figure 2. (**b**) The pattern indexed with the $P6_3mc$ wurtzite structure.

After the buseckite decomposes in the laser beam, the Raman spectrum has bands at 215, 292, 316, 333, 367, 380, and 463 cm^{-1}; there is also a pair of overlapping broad bands in the 540 to 720 cm^{-1} region (Fig. 6b). The most intense bands are at 292, 316, and 367 cm^{-1}.

Interpretation exists for the vibrational spectrum of wurtzite with low-iron content, but it seems to be unavailable for the phase with high-iron contents. The Raman spectrum of 2H ZnS (wurtzite structure) at room temperature has two prominent bands: E_1 (LO) = A_1 (LO) at 351 cm^{-1} and E_1 (TO) = A_1 (TO) at 273 cm^{-1}, and an additional line at 338 cm^{-1} (Zhang et al. 2005). The same features, shifted in wavenumber and less-well resolved, appear in our spectrum (Fig. 6a) of a natural iron-containing wurtzite from Llallagua, Bolivia, of approximate composition $(Zn_{0.43}Mn_{0.31}Fe_{0.26})S$ (Smith et al. 1957). It is likely that the same interpretation of the two dominant bands applies to the meteoritic buseckite.

Although little work is available on wurtzite structure (Zn-Fe)S solid solutions with significant amounts of iron, Osad-chii and Gorbaty (2010) have presented a study of (Zn-Fe)S solid solutions with the sphalerite structure. Their work indicates that the sphalerite Raman spectrum undergoes large changes with increasing iron concentrations, which is in concert with earlier studies they reference that indicate significant changes occur in other sphalerite properties with increasing iron content. In particular, new bands appear at lower Raman shift and band intensities change notably and non-linearly due to a percolation transition in which clusters of Fe form and grow as iron content increases.

The Raman spectrum of rudashevskyite (Fe,Zn)S from the Indarch meteorite (an EH4 enstatite chondrite), for comparison, consists of a broad band that curve-fitting indicates consist of two components centered at about 296 and 326 cm^{-1} (Fig. 6a). The spectrum was obtained at low-laser power to avoid visually obvious decomposition of this phase.

OCCURRENCE AND ASSOCIATED MINERALS

The position of the type material within the Zakłodzie meteorite is not known, although the presence of keilite argues against the sample being from the central portion of the meteorite (Karwowski et al. 2007). Buseckite occurs with enstatite, plagioclase, troilite, sinoite, quartz, tridymite, low-Ni iron (formerly known as "kamacite"), martensitic iron, schreibersite, keilite, and graphite in the Zakłodzie meteorite (Fig. 1) and grains are found in contact with two or more of enstatite, plagioclase, troilite, sinoite, tridymite, and quartz. Troilite in contact with buseckite has a formula of $(Fe_{0.86}Cr_{0.06}Mn_{0.02}Ti_{0.02})S$ (Table 1). All observed buseckite grains are in contact with plagioclase with compositions ranging from mostly K-rich albite $(An_{2.2}Ab_{85.1}Or_{12.7}$ where An, Ab, and Or refer to $CaAl_2Si_2O_8$, $NaAlSi_3O_8$, and $KAlSi_3O_8$ components in the feldspar) to, rarely, low-K, moderately calcic plagioclase $(An_{20.9}Ab_{76.6}Or_{2.5})$. One or both of enstatite and silica are in contact with each of the buseckite grains but alloys (mainly low-Ni iron, plus trace martensitic iron), which comprise roughly 20 vol% of the meteorite (Przylibski et al. 2005), are not observed in contact with buseckite. The alloys are mainly low-Ni iron $(Fe_{0.92}Ni_{0.06}Si_{0.03})$ plus trace amounts of martensitic iron $(Fe_{0.82}Ni_{0.15}Si_{0.03})$, a fine-grained alloy with a bcc α_2 structure. Rare keilite, identified by EBSD, which is also not observed in contact with buseckite, shows $(Fe_{0.43}Mn_{0.35}Mg_{0.16}Cr_{0.02}Ca_{0.02})S$ (Table 1). Troilite $[(Fe_{0.86}Cr_{0.07}Mn_{0.02}Ti_{0.01})S$; Table 1] is a minor phase in Zakłodzie with no significant grain-to-grain differences in chemistry. Przylibski et al. (2005) observed oldhamite (CaS) in Zakłodzie, generally associated with low-Ni iron. Oldhamite was not observed in this study.

Using EBSD and/or Raman, we determined that three silica polymorphs are present in Zakłodzie but that most of the grains are tridymite, the only polymorph reported by Kimura et al. (2005). One cristobalite grain was observed in USNM 7607, in contact with low-Ni iron, enstatite, and tridymite containing albite inclusions. Minor quartz occurs in association with sinoite (Si_2N_2O). Glass was not observed. Rare graphite occurs as euhedral inclusions in low-Ni iron with schreibersite. Rare sinoite was found as euhedral lath-shaped crystals included in or in association with buseckite (Fig. 3). More commonly, sinoite crystals (Fig. 7) occur in contact with two or more of low-Ni iron, K-rich albite, troilite, schreibersite, enstatite, and
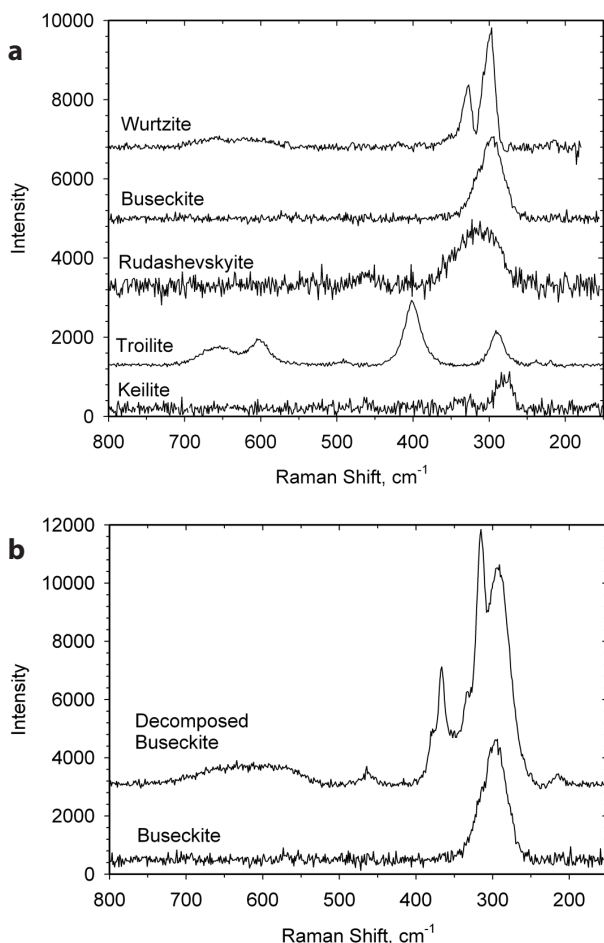
FIGURE 6. (a) Raman spectra of buseckite, troilite, and keilite single crystals from the Zakłodzie meteorite, rudashevskyite from the Indarch meteorite, and wurtzite from Llallagua, Bolivia. (b) Raman spectrum of buseckite obtained under low-laser power (**bottom**) and under high-laser power (**top**). Visible decomposition in the vicinity of the laser spot is observed after the high-laser power run.

quartz. Sinoite was identified by EBSD (Fig. 8) and Raman (Fig. 9). Sinoite's Raman spectrum consists of a strong band centered at 185 cm^{-1}, a medium intensity feature at 544 cm^{-1}, and weaker features at 217, 328, 373, 455, 496, 730, 891, 941, 983, and 1142 cm^{-1}.
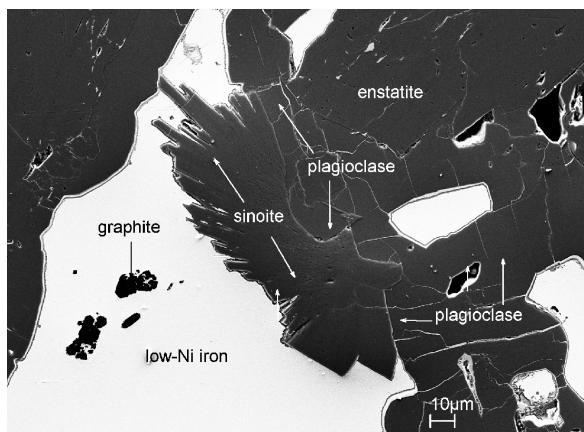

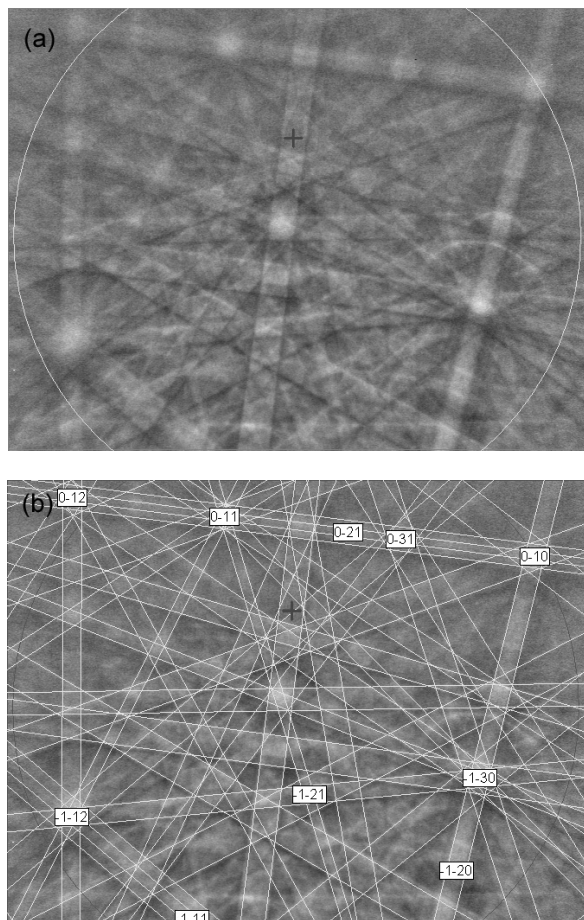**FIGURE 7.** Secondary electron image showing sinoite with low-Ni iron, graphite, enstatite, and plagioclase.

FIGURE 8. (**a**) EBSD pattern of sinoite in Zakłodzie. (**b**) The pattern indexed with the $Cmc2_1$ Si$_2$N$_2$O structure.
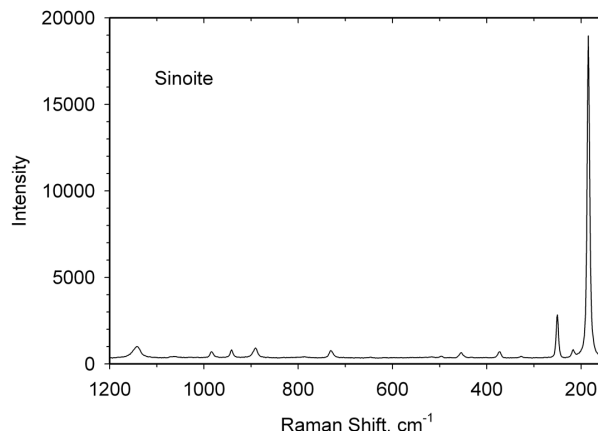

FIGURE 9. Raman spectrum of sinoite from the Zakłodzie meteorite.

ORIGIN AND SIGNIFICANCE

Buseckite [(Fe,Zn,Mn)S with the $P6_3mc$ wurtzite-group structure] is the Fe-dominant analog of wurtzite, a new member of the wurtzite group, joining the Fe-dominant meteoritic mono-sulfide minerals troilite (FeS with a $P6_3/mmc$ structure), keilite [(Fe,Mn,Mg)S with the $Fm3m$ galena-group structure] and ruda-shevskyite [(Fe,Zn)S with the $F\bar{4}3m$ sphalerite-group structure], all of which occur in enstatite-rich meteorites. To consider the origin of buseckite, one must first define the context offered by the host meteorite. Zakłodzie contains euhedral to subhedral, polysynthetically twinned, very low-Mn enstatite crystals that sometimes intrude into metal (i.e., the alloy was molten at the time), igneous graphite, a high-modal content of metal and sulfide (20 and 10% by volume in outer portions of the meteorite), pos-sible relict chondrules, and strongly zoned plagioclase (Przylibski et al. 2005). These features are consistent with an igneous origin for the silicates and fast cooling, suggesting an impact melt with rapid cooling (see Burbine et al. 2000; Keil 2007, 2010; McCoy et al. 1995 for discussion), although Przylibski et al. (2005) pre-ferred a melting event within the parent body followed by rapid cooling. The silicate mode in Zakłodzie is roughly 90 vol% en-statite, and 8% feldspar with accessory relict olivine enclosed in enstatite and accessory silica. Also, Przylibski et al. (2005) noted, based on the MgO-SiO$_2$ system, that liquidus temperatures, and hence peak temperatures for the silicate assemblage in Zakłodzie would have exceeded ~1550 °C. Actual liquidus temperatures for the silicates in Zakłodzie are somewhat lower because the addition of feldspar lowers the liquidus temperature relative to expectations based on MgO-SiO$_2$ but the temperatures are still quite high, roughly 1500 °C according to the ternary systems forsterite-silica-anorthite and forsterite-silica-albite (Anderson 1915; Schairer and Yoder 1961). Olivine is the liquidus phase but it would have been in a reaction relationship with the melt once enstatite, the second silicate, began to crystallize. The crystalliza-tion sequence for fractional or equilibrium crystallization would have been forsterite → enstatite (olivine resorbed) → (silica → feldspar) or (feldspar → silica), with the order of feldspar and silica dependent on the feldspar composition. This is consistent with observed phase assemblages in Zakłodzie as given by Pr-

zylibski et al. (2005). Enstatite is euhedral to subhedral, olivine survives as rounded inclusions in enstatite, and feldspar occurs interstitially between enstatite laths. Silica is usually encountered as rounded, rare inclusions in sulfide in the sample studied by Przylibski et al. (2005) and as mostly rounded tridymite grains independent of sulfides in this study. The occurrence of tridymite is consistent with crystallization of silica near the silicate solidus [1062–1223 °C for equilibrium in the forsterite-silica-plagioclase system (Anderson 1915; Schairer and Yoder 1961) and, presumably, lower in Zakłodzie due to relatively rapid cooling]. The rounded form may, however, indicate partial dissolution and this suggests that silica goes into a reaction relationship at low temperatures, presumably with metallic/sulfide liquids.

Rubin (1983) observed a K-enriched spherule of roughly the same composition ($Ab_{91}Or_9$) as the potassic feldspars in contact with buseckite ($An_2Ab_{85}Or_{13}$). Following Wlotzka et al. (1983), this may reflect vapor-feldspar (or melt) Na-K exchange associated with an impact. Rare quartz grains are consistently associated with sinoite where it is not completely enclosed in sulfide or metal. Hence we suggest that these crystals formed at subsolidus temperatures, where quartz was the stable polymorph of silica, through the oxidation of sinoite (e.g., $Si_2N_2O + 3/2 \, O_2 = 2SiO_2 + N_2$). The origin of the sinoite is uncertain but its occurrence in alloys and sulfides would be consistent with the exsolution of N and Si from the opaque phases, as suggested by Rubin (1997). The cristobalite grain is also a special case. Cristobalite is the stable 1 atm polymorph of silica only above ~1470 °C (e.g., Swamy et al. 1994), which suggests peak temperatures exceeding this value. However, silica is a late-crystallizing phase for the Zakłodzie bulk composition according to the relevant phase diagrams so that tridymite, which is the dominant silica polymorph in Zakłodzie, would be the expected igneous silica and not cristobalite. Moreover, any preexisting silica would have been dissolving into the melt at temperatures above 1200 °C, which for relict silica, implies a relatively short thermal event, especially near peak temperatures because dissolution rates become very fast (e.g., Liang 1999; Shaw 2006). In addition, silica grains are not found as inclusions in enstatite as might be expected were there relict grains that did not completely dissolve during heating. The inclusion of albite, a low-temperature igneous phase, in the cristobalite grain also suggests a relatively low-temperature origin for the grain, again inconsistent with expectations for a grain produced at temperatures above ~1470 °C. One possible scenario by which the cristobalite grain could have formed is that silica, in some rare cases, crystallized as cristobalite and then transformed to tridymite, a sequence that is often observed for quartz in fluxes (e.g., Stevens et al. 1997). Regardless of the history of the cristobalite grain, Zakłodzie's silicates heating to peak temperatures above ~1500 °C followed by rapid cooling.

The opaque phases can also place some constraints on igneous history. The presence of igneous graphite argues for temperatures exceeding ~1150–1200 °C, based on the Fe-Ni-C phase diagram (Gabriel et al. 1987). High-temperature phase relations for the opaque assemblage can be treated, ignoring graphite and minor Mn-Zn-Ca sulfides, in terms of the Fe-Ni-S system. From the mode of 20 vol% alloy and 10% sulfide in Zakłodzie, assuming average densities of 8 and 5 g/cm³, respectively, and assuming that the sulfide is dominated by troilite, we obtain a bulk com-

position of ~81 mol% Fe, 4% Ni, and 14% S. According to the model of Waldner and Pelton (2004) for the Fe-Ni-S system, the liquidus for this bulk composition is ~1350 °C, well below peak temperatures for the silicate melting event and consistent with alloys and sulfides occurring interstitially between silicates.

Based on Fe-Ni-S, Fe-Ni alloys would be the highest temperature opaque phase in Zakłodzie, initially appearing at ~1350 °C, if at equilibrium (Waldner and Pelton 2004), but no sulfides would crystallize above 1000 °C (i.e., sulfides form at temperatures well below the solidus for silicates). At high temperatures, Zn, along with other minor elements such as Cr, Ti, and Mn, is likely accommodated in pyrrhotite so that a separate Zn-rich phase does not form initially. However, pyrrhotite breaks down at lower temperatures and the sulfides troilite, alabandite, keilite, and niningerite, so produced, have no significant solubility for Zn. Daubréelite, a Cr sulfide, can accommodate considerable Zn (e.g., Lin and El Goresy 2002) but this phase is not observed in Zakłodzie. Apparently, under the relatively high temperatures of equilibration for Zakłodzie, keilite and troilite were able to the accommodate Cr, as would be expected based on the Fe-Cr-S system (e.g., Raghavan 1988), and cooling was sufficiently fast so that exsolution of Cr-rich phases such as daubréelite did not occur. The lack of a sulfide with a significant solubility for Zn ultimately led to the formation of buseckite, probably as a breakdown product of pyrrhotite or troilite. This scenario would be consistent with the observed association of troilite with buseckite in Zakłodzie.

Keil (2007) suggests an impact melt origin for Zakłodzie due to the presence of keilite, which he asserts forms upon cooling due to the reaction of alabandite or niningerite with troilite. The expectation is that, in slowly cooling environments such as might be expected in a metamorphic rock or in a slowly cooled igneous rock, sulfides would have equilibrated to very low temperatures, whereas those observed in aubrites and enstatite chondrite impact melt breccias exceed ~500 °C, based on data of Skinner and Luce (1971) and Tauson and Chernyshev (1978). Karwowski et al. (2007) found that Zakłodzie keilites equilibrated down to 500–600 °C. This provides a likely approximate temperature range for which chemical exchange between buseckite and troilite also ceased and it provides a significant line of evidence for rapid cooling rates since Skinner and Luce (1971) and others (e.g., Scott and Barnes 1972) were readily able to achieve equilibrium at these temperatures among metal, troilite, and (Ca,Mg,Mn,Fe) monosulfides in days to months. Although an impact melt, as envisioned by Keil (2007) is a plausible mechanism by which high-equilibration temperatures might be expected for the sulfides, the breakup of a still warm (very hot for Zakłodzie) parent body, as is sometimes evoked for ordinary chondrites (e.g., Scott and Rajan 1981), could potentially also lead to fast cooling from the high temperatures extant within a pre-disrupted parent body. To generate the very high-internal temperatures necessary to explain the observed silicates in Zakłodzie, however, large scale differentiation of metal/sulfide from silicate melt would be expected and this is not observed. Late shock heating could also lead to partial resetting of sulfides but there is little evidence for extensive shock of this meteorite and such an event would not affect the high temperature, fast cooling environment required by the silicates. We conclude, in agreement with Keil (2007),

that Zakłodzie is most likely the result of impact melting of an enstatite enriched precursor material.

Britvin et al. (2008) showed that Fe-dominant Zn-rich monosulfides in Indarch (EH4) have the cubic $F\bar{4}3m$ sphalerite structure, whereas we show in this work that the Fe-dominant Zn-rich monosulfides in Zakłodzie are buseckite ($P6_3mc$ wurtzite structure), a difference in structure that reflects differences in composition and formation conditions. In general, for a given bulk composition, the $P6_3mc$ wurtzite structure is the stable structure at high temperatures and the $F\bar{4}3m$ sphalerite structure is stable at lower temperatures. Although generally treated as a monosulfide, sphalerite is slightly metal deficient and wurtzite slightly sulfur deficient relative to a metal/sulfur ratio of 1:1, so that higher sulfur fugacities favor the sphalerite structure (e.g., Scott and Barnes 1972). These principles extend to more complex chemistries. The wurtzite structure is always the high-temperature form and the sphalerite structure associated with the low-temperature form for a fixed bulk composition. The effect of different metals on the transition temperature is, however, quite variable. For pure ZnS, wurtzite is stable relative to sphalerite only above ~1020 °C but the minimum transition temperature drops to as low as ~850 °C in the FeS-ZnS system (Knitter and Binnewies 1999) and to ~820 °C for Ga_2S_3-ZnS (Zhang et al. 1990). Thus, both Fe and Ga stabilize the $P6_3mc$ wurtzite-structured compounds relative to the $F\bar{4}3m$ sphalerite structure. Manganese and Mg are very strong wurtzite structure stabilizers (Brightwell et al. 1984; Tauson et al. 1977). In the MnS-ZnS system, for example, the minimum temperature for a stable wurtzite structure monosulfide is only ~350 °C. This is why the moderate $P6_3mc$ stabilizers Ga and Fe are plotted at one vertex of Figure 4 and the strong $P6_3mc$ stabilizers, Mg and Mn, at another. Other things being equal, Zn-enriched monosulfides plotting well into the interior of Figure 4 (e.g., buseckite from Zakłodzie), are more likely to have the wurtzite structure than are monosulfides plotting closer to the FeS-ZnS join.

Buseckite is relatively Mn rich and, although it owes its name to being a Fe-dominant composition, Mn is more important than Fe for its formation and survival. In the EH4 chondrite Indarch, rudashevskyite formed during relatively low-temperature metamorphism (Britvin et al. 2008). The relatively low Mn contents of these sulfides (Fig. 4) suggest a relatively high temperature for the $P6_3mc$-$F\bar{4}3m$ transition, probably greater than ~800 °C, which is substantially higher than likely peak metamorphic temperatures for this meteorite (e.g., Huss and Lewis 1995). Thus, it is unlikely that buseckite ever formed during the metamorphism of Indarch. In EH3 chondrites, sulfides formed under various planetary and nebular environments and, from Figure 4, there is a cluster of Zn-enriched monosulfide compositions with relatively high Mn+Mg contents. Some of these may be buseckite and, if there is a mixture of buseckite and rudashevskyite, the distribution of structure types among the grains could potentially be used to constrain thermal history, although this cannot be quantified at present. In EL4-6 chondrites, the Zn-rich monosulfides have high Mg+Mn, comparable to concentrations observed in Zakłodzie (Fig. 3). The structure type(s) for these sulfides have not been determined but the high Mn+Mg greatly decreases the rudashevskyite-buseckite inversion temperatures relative to those pertinent to the low-Mn sulfides of Indarch. Overall, high-

formation temperatures, fast cooling rates, to avoid inversion to the sphalerite structure on cooling, high Mn (+Mg) contents to lower the inversion temperature, and low sulfur fugacities are features of chemistry and formation conditions most likely to favor buseckite over rudashevskyite.

REFERENCES CITED

Anderson, O. (1915) The system anorthite-forsterite-silica. American Journal of Science, 39, 309–312.

Armstrong, J.T. (1995) CITZAF: a package of correction programs for the quantitative electron microbeam X-ray analysis of thick polished materials, thin films, and particles. Microbeam Analysis, 4, 177–200.

Brightwell, J.W., Ray, B., and White, S. (1984) Phase-structures of Zn_{1-x}-Mg_xS prepared by reaction of mixed chlorides with H_2S. Journal of Material Science Letters, 3, 951–954.

Britvin, S.N., Bogdanova, A.N., Boldyreva, M.M., and Aksenova, G.Y. (2008) Rudashevskyite, the Fe-dominant analogue of sphalerite, a new mineral: Description and crystal structure. American Mineralogist, 93, 902–909.

Burbine, T.H., McCoy, T.J., and Dickinson, T.L. (2000) Origin of plagioclase-"enriched", igneous, enstatite meteorites. Meteoritics and Planetary Science, 39, A36.

Buseck, P.R. and Holdsworth, E.F. (1972) Mineralogy and petrology of the Yilmia enstatite chondrite. Meteoritics, 7, 429–447.

El Goresy, A. and Ehlers, K. (1989) Sphalerites in EH chondrites: I. Textural relations, compositions, diffusion profiles, and pressure-temperature histories. Geochimica et Cosmochimica Acta, 53, 1657–1668.

Gabriel, A., Gustafson, P., and Ansara, I. (1987) A thermodynamic evaluation of the C-Fe-Ni system. Calphad, 11, 203–218.

Huss, G.R. and Lewis, R.S. (1995) Presolar diamond, SiC, and graphite in primitive chondrites: Abundances as a function of meteorite class and petrologic type. Geochimica et Cosmochimica Acta, 59, 115–160.

Ikeda, Y. (1989) Petrochemical study of the Yamato-691 enstatite chondrite (E3) IV: Descriptions and mineral chemistry of opaque-mineral nodules. Proceedings of the NIPR Symposium on Antarctic Meteorites, 2, 109–146.

Karwowski, L., Kryza, R., and Przylibski, T.A. (2007) New chemical and physical data on keilite from the Zakłodzie enstatite achondrite. American Mineralogist, 92, 204–209.

Keil, K. (2007) Occurrence and origin of keilite, (Fe$_{>0.5}$,Mg$_{<0.5}$)S, in enstatite chondrite impact-melt rocks and impact-melt breccias. Chemie der Erde, 67, 37–54.

——— (2010) Enstatite achondrite meteorites (aubrites) and the histories of their asteroidal parent bodies. Chemie der Erde, 70, 295–317.

Kimura, M., Weisberg, M.K., Lin, Y., Suzuki, A., Ohtani, E., and Okazaki, R. (2005) Thermal history of enstatite chondrites from silica polymorphs. Meteoritics and Planetary Science, 40, 855–868.

Kissin, S.A. (1989) Application of the sphalerite cosmobarometer to the enstatite chondrites. Geochimica et Cosmochimica Acta, 53, 1649–1655.

Knitter, St. and Binnewies, M. (1999) Der Chemische Transport von Mischkristallen in den Systemen MnS/ZnS, FeS/ZnS und FeS/MnS. Zeitschrift für Anorganische Allgemeine Chemie, 625, 1582–1588.

Kullerud, G. (1953) The FeS-ZnS system. A geological thermometer. Norsk Geologisk Tidsskrift, 32, 61–147.

Liang, Y. (1999) Diffusive dissolution in ternary systems: Analysis with applications to quartz and quartzite dissolution in molten silicates. Geochimica et Cosmochimica Acta, 63, 3983–3995.

Lin, Y. and El Goresy, A. (2002) A comparative study of opaque phases in Qingzhen (EH3) and MacAlpine Hills 88136 (EL3): Representatives of EH and EL parent bodies. Meteoritics and Planetary Science, 37, 577–599.

Ma, C. (2011) Buseckite, IMA 2011-070. CNMNC Newsletter No. 11, December 2011, page 2891. Mineralogical Magazine, 75, 2887–2893.

Ma, C. and Rossman, G.R. (2008) Barioperovskite, $BaTiO_3$, a new mineral from the Benitoite Mine, California. American Mineralogist, 93, 154–157.

——— (2009) Tistarite, Ti_2O_3, a new refractory mineral from the Allende meteorite. American Mineralogist, 94, 841–844.

Ma, C., Beckett, J.R., and Rossman, G.R. (2012) Discovery of buseckite, (Fe,Zn,Mn)S, a new mineral in Zakłodzie, an ungrouped enstatite-rich achondrite. 43rd Lunar and Planetary Science Conference, Abstract 1520.

McCoy, T.J., Keil, K., Bogard, D.D., Garrison, D.H., Casanova, I., Lindstrom,

M.M., Berarley, A.J., Kehm, K., Nichols, R.H., and Hohenberg, C.M. (1995) Origin and history of impact-melt rocks of enstatite chondrite parentage. Geochimica et Cosmochimica Acta, 59, 161–175.

Osadchii, E.G. and Gorbarty, Y.E. (2010) Raman spectra and unit cell parameters of sphalerite solid solutions ($Fe_xZn_{1-x}S$). Geochimica et Cosmochimica Acta, 74, 568–573.

Patzer, A., Schlüter, J., Schultz, L., Tarkian, M., Hill, D.H., and Boynton, W.V. (2004) New findings for the equilibrated enstatite chondrite Grein 002. Meteoritics and Planetary Science, 39, 1555–1575.

Przylibski, T.A., Zagożdżon, P.P., Kryza, R., and Pilski, A.S. (2005) The Zakłodzie enstatite meteorite: Mineralogy, petrology, origin, and classification. Meteoritics and Planetary Science, 40, A185–A200.

Raghavan, V. (1988) The Cr-Fe-S (Chromium-Iron-Sulphur) System. In V. Raghavan, Ed., Phase Diagrams of Ternary Iron Alloys, vol. 2, p. 107–120. Indian Institute of Metals, Calcutta.

Rambaldi, E.R., Rajan, R.S., Housley, R.M., and Wang, D. (1986) Gallium-bearing sphalerite in a metal-sulfide nodule of the Qingzhen (EH3) chondrite. Meteoritics, 21, 23–31.

Rubin, A.E. (1983) The Adhi Kot breccia and implications for the origin of chondrules and silica-rich clasts in enstatite chondrites. Earth and Planetary Science Letters, 64, 201–212.

——— (1997) Sinoite (Si_2N_2O): Crystallization from EL chondrite impact melts. American Mineralogist, 82, 1001–1006.

Schairer, J.F. and Yoder, H.S. (1961) The system albite-forsterite-silica. Carnegie Institution of Washington, Yearbook, 60, 141–144.

Scott, E.R.D. and Rajan, R.S. (1981) Metallic minerals, thermal histories and parent bodies of some xenolithic, ordinary chondrite meteorites. Geochimica et Cosmochimica Acta, 45, 53–67.

Scott, S.D. and Barnes, H.L. (1972) Sphalerite-wurtzite equilibria and stoichiometry. Geochimica et Cosmochimica Acta, 36, 1275–1295.

Shaw, C.S.J. (2006) Effects of melt viscosity and silica activity on the rate and mechanism of quartz dissolution in melts of the CMAS and CAS systems. Contributions to Mineralogy and Petrology, 151, 665–680.

Skinner, B.J. and Luce, F.D. (1971) Solid solutions of the type (Ca,Mg,Mn,Fe) S and their use as geothermometers for the enstatite chondrites. American Mineralogist, 56, 1269–1296.

Smith, F.G., Dasgupta, S.K., and Hill, V.G. (1957) Manganoan ferroan wurtzite from Llallagua, Bolivia (I). Canadian Mineralogist, 6, 128–135.

Stevens, S.J., Hand, R.J., and Sharp, J.H. (1997) Polymorphism of silica. Journal of Materials Science, 32, 2929–2935.

Swamy, V., Saxena, S.K., Sundman, B., and Zhang, J. (1994) A thermodynamic assessment of silica phase diagram. Journal of Geophysical Research, 99, 11787–11794.

Tauson, V.L. and Chernyshev, L.V. (1978) The sphalerite-wurtzite transition in isomorphous mixtures of the system ZnS-MnS-CdS-FeS. Geochemistry International, 15(5), 33–41.

Tauson, V.L., Chernyshev, L.V., and Makeyev, A.B. (1977) Phase relations and structural characteristics of mixed crystals in the system ZnS-MnS. Geochemistry International, 14(3), 33–45.

Waldner, P. and Pelton, A.D. (2004) Critical thermodynamic assessment and modeling of the Fe-Ni-S system. Metallurgical and Materials Transactions, 35B, 897–907.

Wlotzka, F., Palme, H., Spettel, B., Wänke, H., Fredriksson, K., and Noonan, A.F. (1983) Alkali differentiation in LL-chondrites. Geochimica et Cosmochimica Acta, 47, 743–757.

Zhang, J.M., Chen, W.W., Ardell, A.J., and Dunn, B. (1990) Solid-state phase equilibria in the ZnS-Ga$_2$S$_3$ system. Journal of the American Ceramic Society, 73, 1544–1547.

Zhang, X., Zhang, Y., Song, Y., Wang, Z., and Yu, D. (2005) Optical properties of ZnS nanowires synthesized via simple physical evaporation. Physica E: Low-Dimensional Systems & Nanostructures (Amsterdam, Netherlands), 28, 1–6.